


## ORIGINAL ARTICLE

# Paclitaxel-based supramolecular hydrogel loaded with mifepristone for the inhibition of breast cancer metastasis

Cui-Cui Zhao<sup>1</sup> | Chuan-Gui Zhang<sup>1</sup> | Xuan Sun<sup>1</sup> | Qingxiang Guo<sup>2</sup> | Jinjian Liu<sup>2</sup> | Yan Liu<sup>1</sup> | Ya-Nan Hao<sup>1</sup> | Guowei Feng<sup>1</sup> | Lijun Yang<sup>2</sup> | Hong Liu<sup>1</sup> | Jianfeng Liu<sup>2</sup> 

<sup>1</sup>Tianjin's Clinical Research Center for Cancer, Key Laboratory of Cancer Prevention and Therapy, Tianjin, Key Laboratory of Breast Cancer Prevention and Therapy, Tianjin Medical University, Ministry of Education, National Clinical Research Center for Cancer, Tianjin Medical University Cancer Institute and Hospital, Tianjin, China

<sup>2</sup>Key Laboratory of Radiopharmacokinetics for Innovative Drugs, Chinese Academy of Medical Sciences, and Institute of Radiation Medicine, Chinese Academy of Medical Sciences and Peking Union Medical College, Tianjin, China

## Correspondence

Hong Liu, Tianjin Medical University Cancer Institute and Hospital, huanhuxi Road, Tianjin 300060, China.  
Email:lh713@163.com

Lijun Yang, and Jianfeng Liu, Institute of Radiation Medicine, Chinese Academy of Medical Science & Peking Union Medical College, Baidi Road 238, Tianjin 300192, China.

Emails: yanglijun@irm-cams.ac.cn; liujianfeng@irm-cams.ac.cn

## Funding information

National Natural Science Foundation of China, Grant/Award Number: 81701840; CAMS Innovation Fund for Medical Sciences, Grant/Award Number: 2016-I2 M-3-022; National Science Fund for Distinguished Young Scholars of Tianjin, Grant/Award Number: 18JCJQC47300; Non-profit Central Research Institute Fund of Chinese Academy of Medical Sciences, Grant/Award Number: 2018PT35031; Major Science and Technology Project for prevention and treatment of major diseases in Tianjin, Grant/Award Number: 19ZXDBSY00090

## Abstract

Breast cancer is the leading cause of cancer death among women and almost all of the breast cancer-caused mortality is related to metastasis. It has been reported that glucocorticoid facilitates the metastasis of breast cancer in mice, and mifepristone can antagonize the effect of glucocorticoid. Paclitaxel is one of the important drugs in the treatment of breast cancer. Mifepristone combined with paclitaxel could be an effective strategy for inhibiting breast cancer metastasis. However, their inherent defects, in terms of short blood circulation half-life and lack of tumor targeting, not only limit their effectiveness but also cause adverse reactions. Therefore, our aim is to explore a novel protocol against breast cancer metastasis, further optimize its therapeutic efficacy by a nanodelivery system, and explore its mechanism. Herein, a paclitaxel-conjugated and mifepristone-loaded hydrogel (PM-nano) was prepared by self-assembly. Its characterizations were studied. The antimetastatic effect was evaluated in vitro and in vivo and its mechanism was also explored by western blot assay. The resultant PM-nano was developed with favorable water solubility and good biocompatibility. Moreover, PM-nano displayed increased cell uptake properties and stimulated drug release in the tumor micro-acidic environment. The PM-nano was more effective in inhibiting the proliferation and metastasis of breast cancer than other groups in vitro and in vivo. The PM-nano might inhibit metastasis through glucocorticoid receptor/receptor tyrosine kinase-like orphan receptor 1 and MMPs. Taken together, PM-nano showed superior antimetastatic effects against breast cancer and excellent biocompatibility in vitro and in vivo, providing a new option for limiting metastasis.

**Abbreviations:** <sup>1</sup>H NMR, proton nuclear magnetic resonance; 4T1-Luc, 4T1-luminescence; CD, circular dichroism; DXM, dexamethasone; FITC@Hydrogel, PM-nano hydrogel loaded with FITC; GR, glucocorticoid receptor; HRMS, high resolution mass spectrometry; M $\beta$ CD, methyl- $\beta$ -cyclodextrin; MIF, mifepristone; Na<sub>2</sub>CO<sub>3</sub>, sodium carbonate; PTX, paclitaxel; PD, PTX + DXM; PM, PTX + MIF; PMD, PTX + MIF + DXM; PM-nano, PTX-conjugated and MIF-loaded supramolecular hydrogel; P-nano, PTX hydrogel; PTX-SA, SA-modified PTX compound; RBC, red blood cell; ROR1, receptor tyrosine kinase like orphan receptor 1; SA, succinic anhydride; TEM, transmission electron microscope; UV-vis, ultraviolet visible.

This is an open access article under the terms of the Creative Commons Attribution-NonCommercial-NoDerivs License, which permits use and distribution in any medium, provided the original work is properly cited, the use is non-commercial and no modifications or adaptations are made.

© 2021 The Authors. *Cancer Science* published by John Wiley & Sons Australia, Ltd on behalf of Japanese Cancer Association.

## KEYWORDS

breast cancer, metastasis, mifepristone, paclitaxel, supramolecular hydrogel

## 1 | INTRODUCTION

Breast cancer is the most common malignancy in the world and the leading cause of cancer death in women.<sup>1</sup> According to the statistics, more than 90% of breast cancer-related mortality is closely related to metastasis.<sup>2</sup> Previous reports have revealed that glucocorticoid (DXM) facilitates the metastasis of breast cancer.<sup>3,4</sup> Glucocorticoid receptor antagonist (MIF) can antagonize the effect of DXM by competitively binding with GR to improve the therapeutic effect of breast cancer.<sup>4-8</sup> In addition, among various drugs, taxanes, such as PTX, are the cornerstone of chemotherapy for the prevention and treatment of breast cancer metastasis.<sup>9</sup> Therefore, the combination of PTX and MIF could be a potential therapeutic strategy for breast cancer metastasis.

However, short blood circulation half-life induced by the inadequate water solubility, poor distribution in tumors, and some side-effects to normal tissues dramatically limited the antitumor effect of PTX and MIF *in vivo*.<sup>9,10</sup> Therefore, solutions to these problems are urgently needed. Numerous researchers have reported that nanomaterials could act as appropriate drug delivery carriers to improve drug bioavailability and decrease adverse effects.<sup>11-16</sup> Among various nanomaterials, nanofiber-structured supramolecular hydrogels are considered to be commendable nanocarriers for anticancer drug delivery because of their simple preparation, controllable drug loading, and high stability.<sup>17</sup>

Based on the above, integrating PTX and MIF into a supramolecular hydrogel could effectively overcome the inherent limitations of the two drugs and effectively inhibit metastasis of breast cancer. Herein, PTX-conjugated and MIF-loaded supramolecular hydrogel (PM-nano) was prepared. It showed improved solubility of the two drugs, favorable biocompatibility, and enhanced tumor inhibition and antimetastatic effects *in vitro* and *in vivo*. The mechanism of inhibiting breast cancer metastasis was also discussed. This simple and effective combination strategy could provide a novel insight into solving practical problems in breast cancer treatment.

## 2 | MATERIALS AND METHODS

### 2.1 | Materials

Paclitaxel, SA, MIF, DXM, pyridine, Na<sub>2</sub>CO<sub>3</sub>, paraformaldehyde, FITC, DAPI, Triton X-100, MTT, and D-luciferin potassium salt were all purchased from Shanghai Macklin Biochemical Co., Ltd. All the solvents, including acetone, methanol, polyoxyethylene castor oil, ethanol, and DMSO were obtained from J&K Scientific Ltd, and used without further purification. DMEM, RPMI-1640, FBS, and penicillin-streptomycin solution were purchased from Gibco Life

Technologies. MCF-7, MDA-MB-231, and 4T1 cells were maintained in our laboratory.

### 2.2 | Synthesis and characterization of SA-modified PTX compound

Succinic anhydride-modified PTX compound was synthesized according to Figure S1. Briefly, PTX (0.5 g) and SA (0.9 g) were dissolved in pyridine (12 mL) and the resultant mixture was stirred at room temperature. Five hours later, the solution was evaporated to dryness and the residue was treated with water (30 mL). After stirring for 0.5 hours, the precipitate was filtered and then dissolved in acetone (10 mL). Water was slowly added and the fine crystal was collected by filtration. The chemical structure of PTX-SA was confirmed by <sup>1</sup>H NMR (Bruker) spectrometry and HRMS (Thermo Finnigan LCQ AD System).

### 2.3 | Preparation of hydrogels

Succinic anhydride-modified PTX compound (4 mg) and MIF (43 μg) were dispersed in 300 μL PBS containing Na<sub>2</sub>CO<sub>3</sub> (445.2 μg). After sonication at room temperature, PM-nano was formed by the self-assembly process. In a similar way, FITC@Hydrogel was prepared by adding FITC, and P-nano was prepared without adding MIF.

### 2.4 | Grouping

In order to verify that combined use of MIF and PTX can enhance the efficacy, and PM-nano can improve the antimetastatic effect, cells and animals were divided into seven groups: one experimental group (PM-nano group), one blank control group (no medications), and five drug control groups (PM group [PTX + MIF], P-nano group, P group [PTX], PD group [PTX + DXM], and PMD group [PTX + MIF + DXM]).

### 2.5 | Characterizations

The size distribution, UV-vis absorption spectra, zeta potential, and CD spectra of hydrogels were measured on a dynamic light scattering spectrometer (BI-200SM; Malvern), UV-vis spectrophotometer (UV-2550; Shimadzu), zeta potential analyzer (ZetaPALS; Brookhaven), and BioLogic (MOS-450) system, respectively. The rheology test was used to study the formation, stability, and viscoelasticity by a rheometer (AR 1500ex; TA Instruments). Moreover, the micromorphology

was characterized by TEM. Then PM-nano was dispersed and incubated in serum at 37°C for 24 hours. The mixture was imaged by TEM at the predetermined time point to evaluate the structure stability.

## 2.6 | Drug release and uptake in vitro

Drug release of PM-nano hydrogel was determined by dialysis and HPLC. After treated with free FITC or FITC@Hydrogel for 4 hours, the fluorescence intensity in breast cancer cells were semiquantitatively analyzed by ImageJ software. The contents of free PTX, free MIF, and PM-nano in breast cancer cells were measured by HPLC after incubating 4 hours with free MIF, free PTX, or PM-nano [Correction added on 4 February 2022, after first online publication: In section 2.6 of Materials and Methods, the phrase 'after incubating 24 hours with PM-nano or PM' in the third sentence was corrected to 'after incubating 4 hours with free MIF, free PTX, or PM-nano' in this version.] The internalization of PM-nano in 4T1 cells was then investigated by TEM after 4 hours of incubation. The cellular uptake mechanism was also studied by quantifying the intracellular concentration of PTX with HPLC after incubation with PM-nano, M $\beta$ CD, amiloride, and chlorpromazine.

## 2.7 | Biocompatibility and pharmacokinetics

The RBC suspension was incubated with the materials for 3 hours at 37°C to study the hemolysis ratio of PM-nano. Hematological analysis of mice was undertaken on days 1 and 7 after treatment. In order to study the pharmacokinetics, the drug concentration in the venous blood of rats and in the tumor, heart, liver, spleen, lung, and kidney of 4T1-bearing mice treated with materials were determined by liquid chromatography-tandem mass spectrometry (LCMS-8060; Shimadzu) at given time points.

## 2.8 | Functions of drugs in vitro

Briefly, after the materials and cells were coincubated for 0, 6, 12, and 24 hours, photographs were taken by a light microscope (Leica) and the scratch areas were measured using ImageJ software. The wound healing percentage (%) = (scratch area at 0 hour – scratch area of appointed time) / scratch area at 0 hour  $\times$  100%. In the Transwell invasion assay, the cells that migrated to the bottom of the filter membrane were fixed, stained, imaged, and counted after coincubation for 24 hours. Moreover, after the cells were treated with materials for 24 hours, MTT and DMSO were added. The optical density was measured at 490 nm by a microplate reader. The cell survival rates were calculated, and IC<sub>50</sub> values were calculated with GraphPad Prism 5 software. The expression of ROR1 (Abcam),  $\beta$ -actin (Proteintech), MMP2 (Wanleibio), and MMP9 (Wanleibio) in PM-nano, PD, and control group were shown by Imager Lab software in the western blot assay.

## 2.9 | Functions of drugs in vivo

The mice were purchased from Beijing Vital River Laboratory Animal Technology Co., Ltd. The experimental protocol was approved by the Animal Care Committee of Chinese Academy of Medical Sciences and was in compliance with the guidelines for animal experiments and the provisions of the Declaration of Helsinki. One million 4T1-Luc cells were injected into the mammary fat pad of each healthy 6-week-old female BALB/c mouse. When tumors grew to approximately 100 mm<sup>3</sup>, which was defined as the first day of treatment, the mice were randomly divided into seven groups (n = 8) for material treatment, measurement, in vivo bioluminescence imaging, euthanasia, anatomy, and H&E staining. Tumor volume (mm<sup>3</sup>) = length  $\times$  width<sup>2</sup>/2. The mice were killed when the tumor volume reached 2000 mm<sup>3</sup> or on day 21.

## 2.10 | Statistical analysis

SPSS 22.0 software was used for statistical analysis. All data are shown as mean  $\pm$  SD. The statistical significance of difference was determined by Student's *t* test, and *P* < .05 was defined as statistically significant.

## 3 | RESULTS

### 3.1 | Preparation of hydrogels

The hydrogelator PTX-SA was synthesized through the esterification of PTX and SA (Figure S1), and confirmed by <sup>1</sup>H NMR (Figure S2) and HRMS (Figure S3). We successfully prepared stable supramolecular hydrogel consisting of PTX-SA and MIF (PM-nano) after simple sonication, and used PTX-SA alone to form hydrogel (P-nano) as a control (Figure 1Aa,b). After water was added, the hydrogels could be transformed into clear and homogeneous solutions (Figure 1Aa',b'). In comparison, the free PTX solution (with the same PTX concentration as PM-nano) and the free MIF solution (with the same MIF concentration as PM-nano) were turbid and not homogeneous (Figure 1Ac',d').

### 3.2 | Characterizations of hydrogels

As shown in Figure S4, the average hydrodynamic size of the PM-nano was 67.6  $\pm$  6.6 nm, which was a little larger than that of P-nano (61.3  $\pm$  5.2 nm). Free PTX-SA and free MIF showed maximum absorption peaks at approximately 225 nm and 310 nm, respectively (Figure S5A). They were almost superimposed with the spectra of PM-nano, providing evidence for the successful loading of MIF on the PTX-SA-based nanofibers. Figure S5B shows the zeta potential of P-nano was -14.6  $\pm$  2.9 mV as a result of the carboxyl and hydroxy groups in the PTX-SA molecules. After being loaded with MIF, the

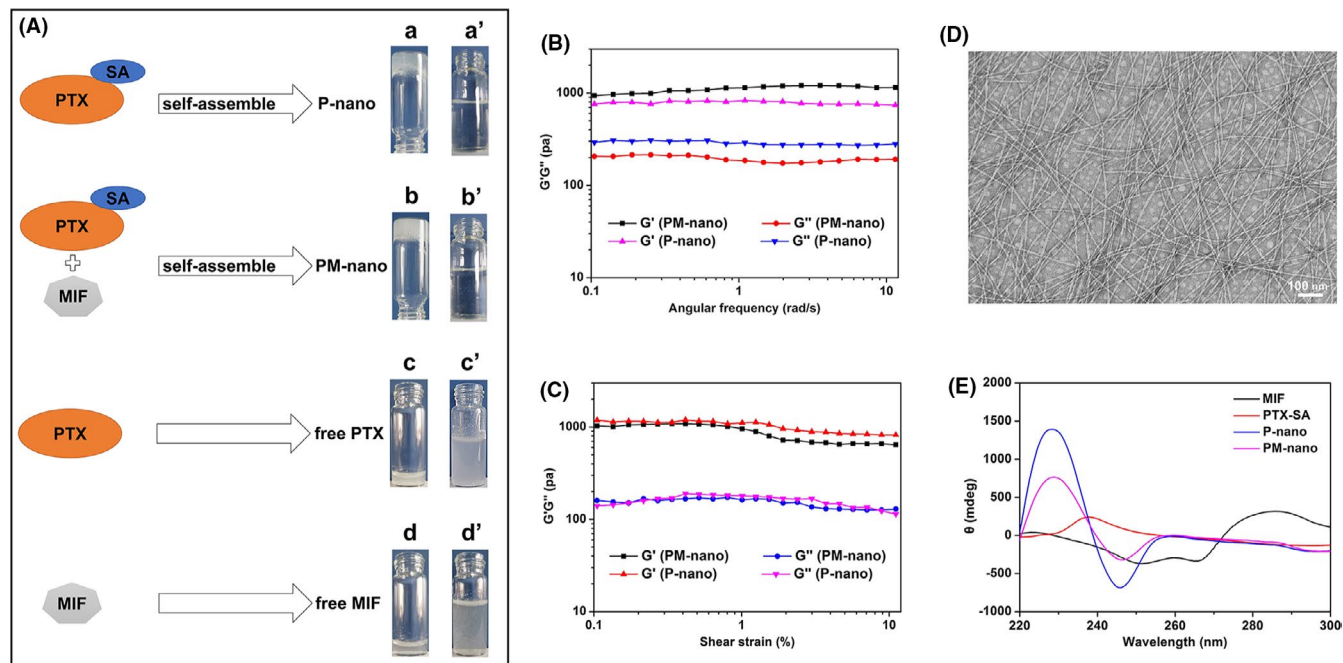


**FIGURE 1** Characterizations of paclitaxel (PTX)-conjugated and mifepristone (MIF)-loaded hydrogel (PM-nano) and PTX hydrogel (P-nano). A, Photographs of P-nano hydrogel, PM-nano hydrogel, free PTX solution with the same PTX concentration as PM-nano, and free MIF solution with the same MIF concentration as PM-nano before (a, b, c, d) and after (a', b', c', d') the addition of equal volume of water. B, Angular frequencies of PM-nano and P-nano. C, Shear strains of PM-nano and P-nano. D, Transmission electron microscopy images of PM-nano. E, Circular dichroism spectra of succinic anhydride (SA)-modified PTX compound (PTX-SA), MIF, PM-nano, and P-nano

zeta potential of PM-nano was decreased to  $-17.7 \pm 1.7$  mV due to the hydroxy groups in the loaded MIF molecules.

Rheology tests (Figure 1B,C) showed that the curves of storage moduli ( $G'$ ) were always higher than those of loss moduli ( $G''$ ) for both PM-nano and P-nano, further demonstrating the formation of the two hydrogels. In addition, the value of  $G'$  and  $G''$  displayed weak frequency dependence and strain dependence, indicating the good stability and high viscoelasticity of the hydrogels. The micro-morphology was characterized by TEM. As shown in Figures 1D and S6, there were plenty of nanofibers with micrometer length in the TEM images and they formed a dense net structure by winding with each other. Although the nanofibers gradually became shorter and thinner with the prolongation of coincubation time, a large number of small fibers still existed in the serum after 10 hours of incubation (Figure S7), suggesting the favorable stability of PM-nano in the blood. The CD spectra (Figure 1E) revealed that the absorption spectra of MIF solution and PTX-SA solution were ruleless, suggesting the random distribution of these two free molecules. However, PM-nano and P-nano both showed a positive peak at approximately 229 nm and negative peak near 246 nm, indicating that a typical  $\beta$ -sheet conformation in the nanofibers and the loading of MIF did not disrupt the inner order of the secondary structure.

### 3.3 | Drug release and uptake in vitro

The drug release behavior of PM-nano under different pH conditions was investigated through HPLC. As shown in Figure 2A, at pH

7.4, which simulated normal physiological conditions, only 53.1% of loaded PTX and 56.9% of loaded MIF was released from the PM-nano after incubation for 48 hours at 37°C, whereas the release rate of the two drugs was significantly accelerated at pH 5.5 (81.4% for PTX and 91.6% for MIF). Figures 2B, S8, and S9 showed FITC@Hydrogel had more distinct green fluorescence than free FITC in MCF-7 and MDA-MB-231 cells. Similarly, the amount of PM-nano measured by HPLC in each breast cancer cell was approximately 2-3-fold higher than that of free drugs (Figure 2C,D). As shown in Figure S10, nanofiber aggregates and flexuous nanofibers were observed in the lysosome and cytoplasm, respectively, of cells treated with PM-nano, suggesting that PM-nano could be smoothly internalized by tumor cells. In addition, the cellular uptake of PM-nano at 4°C was almost one-tenth of that at 37°C (Figure S11). With the addition of M $\beta$ CD during the cellular uptake process, the intracellular PM-nano concentration dramatically decreased to 16.9% compared with that of the cells free of endocytosis inhibitor treatment.

### 3.4 | Biocompatibility and pharmacokinetics

As shown in Figure 3A,B, there was inappreciable hemolytic phenomenon after the incubation of RBCs with PM-nano and P-nano; even at the highest concentration (0.5 mg/mL), their hemolysis ratios were clearly lower than other groups. Subsequently, hematology analysis was undertaken on mice at the days 2 and 8 after intravenous injection. All the hematological indicators were in normal ranges and displayed no obvious variations after treatment (Figure 3C).

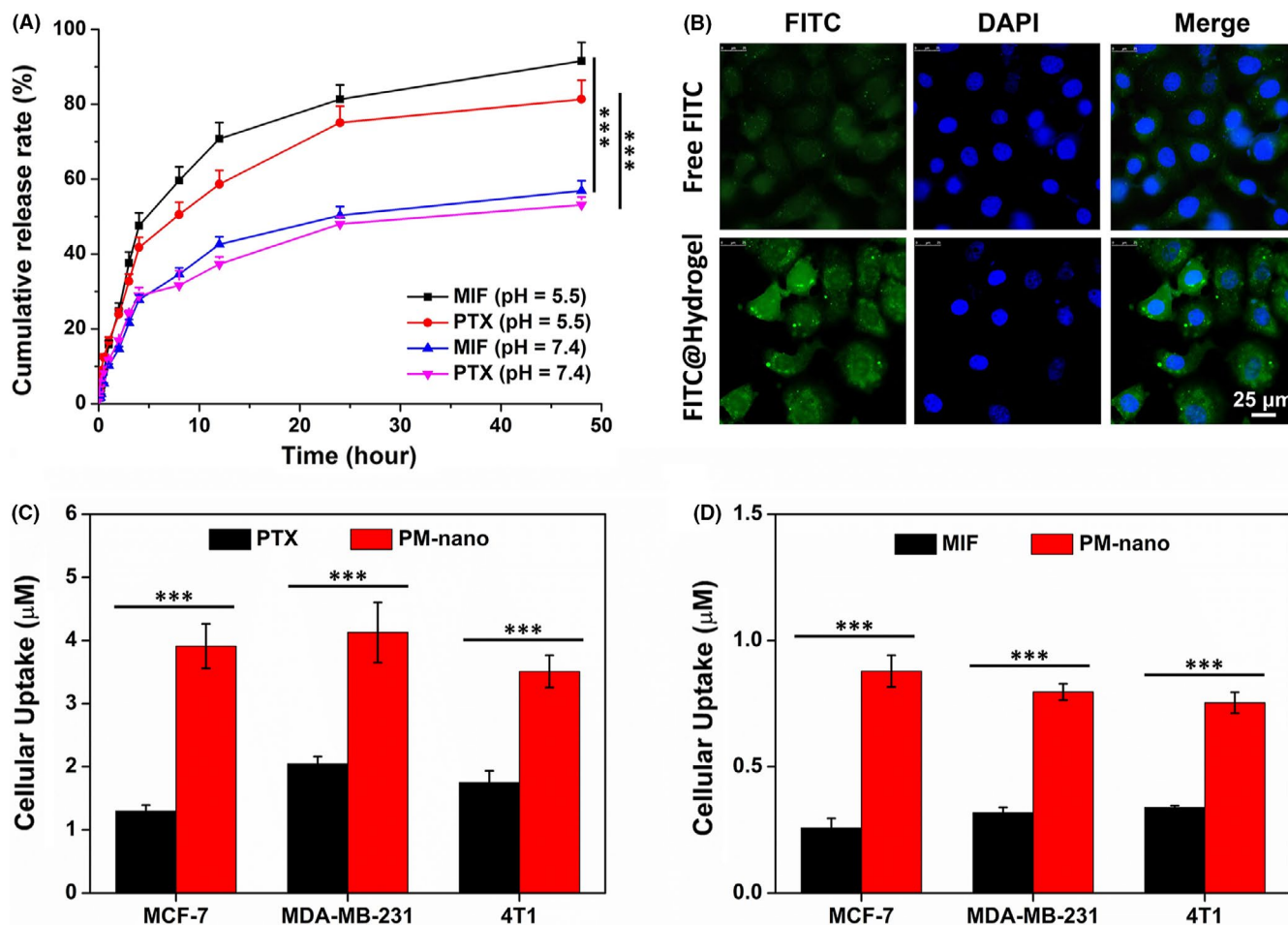


**FIGURE 2** Drug release in vitro and cellular uptake of paclitaxel (PTX)-conjugated and mifepristone (MIF)-loaded hydrogel (PM-nano) in breast cancer cells. A, Drug release of PM-nano in PBS with different pH values (7.4 and 5.5, simulated normal physiological conditions and tumor micro-acidic environment, respectively). B, Fluorescence images of MDA-MB-231 cells treated with free FITC or FITC-loaded PM-nano hydrogel (FITC@Hydrogel) after incubation at an equivalent FITC concentration (10  $\mu\text{g}/\text{mL}$ ) for 4 h (green, FITC; blue, DAPI). C, D, Cellular uptake amounts of PTX (C) and MIF (D) in breast cancer cells evaluated by HPLC after 4 h of incubation with free MIF, free PTX, or PM-nano. \*\*\* $P < .001$

Figure 4A,B shows that the concentration of the two free drugs both declined rapidly with the blood circulation  $t_{1/2}$  of  $3.21 \pm 0.38$  and  $5.83 \pm 0.97$  hours for free PTX and free MIF, respectively. However, after being encapsulated into the hydrogel, the retention time of the loaded PTX ( $t_{1/2} = 9.89 \pm 1.12$ ) and MIF ( $t_{1/2} = 9.06 \pm 0.89$  hours) in the blood was significantly prolonged, indicating the enhanced blood circulation capability of PM-nano.

As presented in Figure 4C-F, PTX and MIF were mainly distributed in the liver and kidney of mice after treatment, indicating the hepatorenal metabolic pathways of the two free drugs. However, PM-nano tended to deposit in the liver, spleen, and lung. Moreover, after being encapsulated into the hydrogel, the concentration of the two drugs in the tumor was remarkably increased due to their prolonged blood circulation  $t_{1/2}$  and the enhanced permeability and retention effect of nanomaterials. Notably, the hydrogel-loaded PTX and MIF showed similar biodistribution in tumor-bearing mice.

### 3.5 | Antitumor effect in vitro

The cell scratch assay was undertaken to investigate the antimigration effect of PM-nano. As seen in Figures 5A-C and S12A, the scratch areas showed different degrees of reduction after treatments; PM-nano showed the largest scratch area compared with other groups, signifying the smallest wound healing percentage and most prominent antimigration effect. Furthermore, the anti-invasion effect was evaluated by cell invasion assay. The number of cells passing through the membrane from the upper chamber to the lower chamber in the PM-nano group was the least of all groups (Figures 5D-F and S12B), indicating that PM-nano had the strongest inhibitory effect on the invasion of breast cancer cells. As shown in Figures 5G,H and S12C, the survival rate of breast cancer cells was obviously concentration-dependent. The cell viability of PM-nano was lowest among all groups. The corresponding  $\text{IC}_{50}$  values of PM-nano were the lowest compared with other groups.



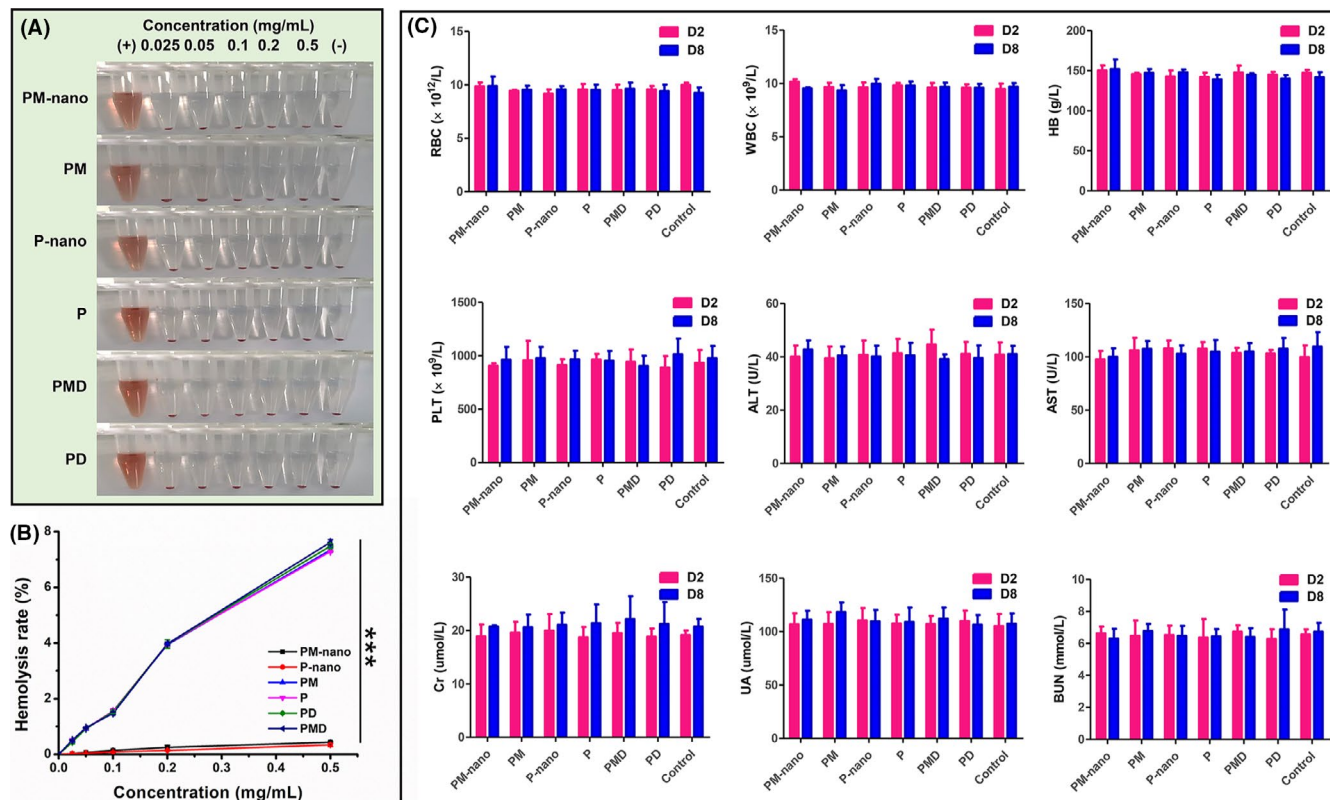


**FIGURE 3** Biocompatibility of paclitaxel (PTX)-conjugated and mifepristone (MIF)-loaded hydrogel (PM-nano). A, Hemolysis photographs after incubation with 2% red blood cell (RBC) suspension and various materials. B, Hemolysis ratios in the PTX concentration range of 0–0.5 mg/mL. C, Hematology analyses of mice on day 2 (D2) and D8 of treatment. \*\*\* $P < .001$ . ALT, alanine aminotransferase; AST, aspartate aminotransferase; BUN, blood urea nitrogen; Cr, creatinine; P, paclitaxel; PD, PTX + dexamethasone; HB, hemoglobin; PLT, platelets; PM, PTX + MIF; PMD, PTX + MIF + dexamethasone; P-nano, PTX hydrogel; UA, uric acid; WBC, white blood cells

Thus, PM-nano had the maximum inhibition of cell proliferation among all groups.

Moreover, the wound healing percentage, number of cells passing through the Transwell membrane, and cell viability in the P and PMD groups were similar, indicating that they had the same antitumor activity against breast cancer cells. They were smaller than those of the PD and control groups, and larger than those of the PM and P-nano groups.

### 3.6 | Western blot assay

It has been reported that glucocorticoid can upregulate ROR1 and promote breast cancer metastasis.<sup>4</sup> Both MMP2 and MMP9 are closely related to breast cancer metastasis.<sup>18,19</sup> Thus, western blot analysis was used to explore the underlying antimetastatic mechanism by measuring the expression of ROR1, MMP2, and MMP9 after different treatments. As shown in Figure 5I, PM-nano and PD both clearly decreased the expression of ROR1, MMP2, and MMP9 compared with the control group, but the extent of reduction with PM-nano was more pronounced.

### 3.7 | Antitumor and antimetastatic effect in vivo

Based on the above results, 4T1-Luc cells were chosen to establish orthotopic breast cancer tumor-bearing mouse models that evaluated the antitumor and antimetastatic activity in vivo. After treatment for 21 days, all mice were alive. The PM-nano group showed the slowest tumor growth rate and the smallest tumor size among all groups (Figure 6A,B). The body weight of mice after different treatments was almost the same (Figure 6C).

As shown in Figure 7A, each mouse in the PM-nano group had only one tumor fluorescence signal at the original inoculation site, whereas in other groups, more than one tumor fluorescence signal was observed at other sites in addition to the signal at the original inoculation site, indicating no breast cancer metastasis in mice of the PM-nano group. Although no obvious ischemia, necrosis, or fibrosis was found by pathology analysis, the organs suffered from obvious tumor metastasis in the PBS group, and no metastasis was observed in PM-nano group (Figure 7B,C). The extent of metastases revealed by pathology analysis and bioluminescence imaging of small animals was basically consistent (Figure 7D,E). It is worth noting that there were some metastases to organs such as heart, spleen, kidney, and

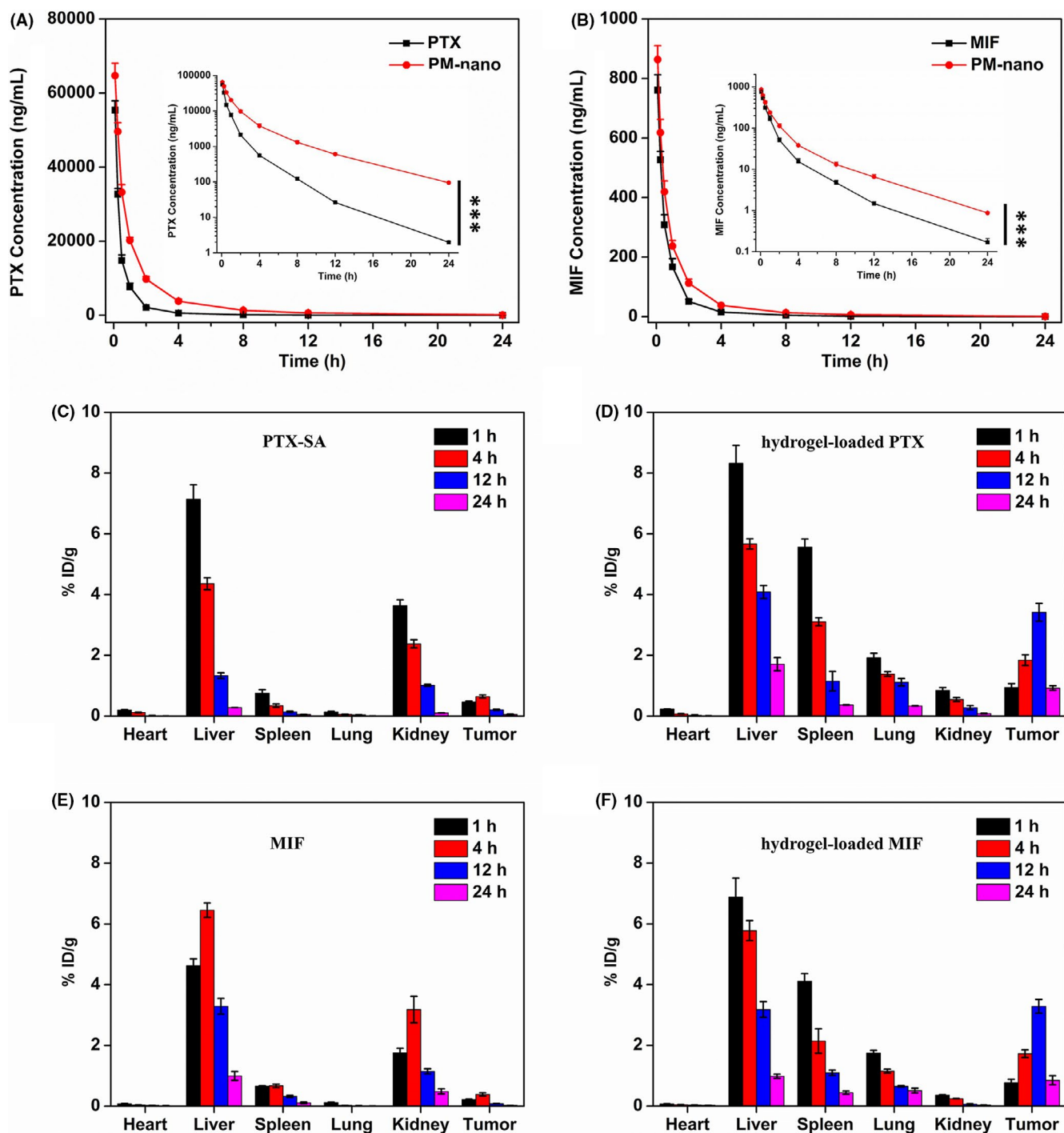


**FIGURE 4** Pharmacokinetics of paclitaxel (PTX)-conjugated and mifepristone (MIF)-loaded hydrogel (PM-nano). A, B, Blood clearance curves of free PTX and hydrogel-loaded PTX (A), and free MIF and hydrogel-loaded MIF (B). C-F, Biodistribution of free PTX (C), hydrogel-loaded PTX (D), free MIF (E), and hydrogel-loaded MIF (F) at various time points after treatment.\*\*\*  $P < .001$ . PTX-SA, succinic anhydride-modified PTX compound

adrenal gland, in addition to the more common metastatic sites of lung, liver, and lymph node (Figure 7F).

## 4 | DISCUSSION

Herein, the solubility of PTX and MIF was significantly improved after the formation of hydrogels. According to previous reports,

the water solubility of PTX was no more than  $0.1 \text{ mg/mL}$  ( $117 \mu\text{mol L}^{-1}$ ).<sup>20</sup> In contrast, the concentrations of PTX in P-nano and PM-nano were  $13.5 \text{ mmol L}^{-1}$ , approximately 110 times higher than that of free PTX, indicating that our supramolecular hydrogel could significantly improve the PTX solubility. In addition, in clinical practice, the solubility of PTX was increased by the addition of cosolvents, which usually induced some adverse reactions.<sup>20</sup> Although the administration of histamine receptor antagonists and glucocorticoids reduced

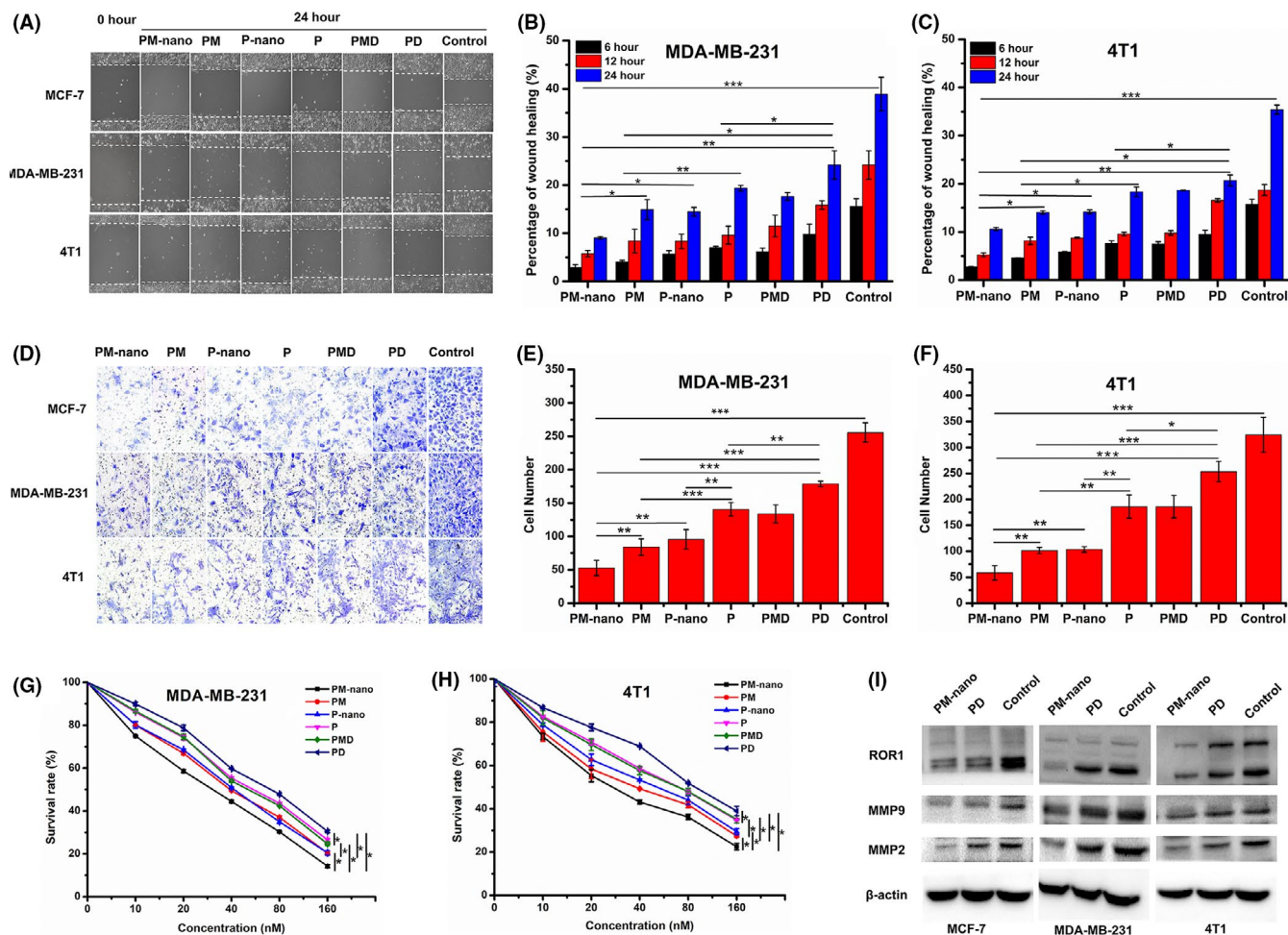


**FIGURE 5** Effects on the biological functions of breast cancer cells. A–C, Images and quantification analysis of cell scratch assays before and after 24 h of treatment with various materials. D–F, Images and quantification analysis of invaded cells in Transwell assays. G, H, Cytotoxicity of various materials against MDA-MB-231 cells and 4T1 cells evaluated by MTT assays. I, Western blots of receptor tyrosine kinase like orphan receptor 1 (ROR1), MMP9, and MMP2 in different cells after various treatments. \* $P < .05$ , \*\* $P < .01$ , \*\*\* $P < .001$ . P, paclitaxel; PD, paclitaxel + dexamethasone; PM, paclitaxel + mifepristone; PMD, paclitaxel + mifepristone + dexamethasone; PM-nano, paclitaxel-conjugated and mifepristone-loaded supramolecular hydrogel; P-nano, paclitaxel hydrogel

the cosolvent-related adverse reactions before the application of PTX, the allergic reaction cannot be completely eliminated.<sup>4</sup> In our hydrogel, PTX had the dual function of chemotherapy drug and carrier. Therefore, PM-nano not only enhanced the solubility but also avoided the adverse reactions caused by cosolvents and other carrier components, and provided more possibilities for combination regimens containing PTX to inhibit the metastasis of breast cancer.

The characterization results clearly showed that both PM-nano and P-nano had nanofiber structures with good stability and high viscoelasticity, which made them easier to be internalized by cancer cells.<sup>13,15,21</sup> The release rates of PTX and MIF were significantly increased at pH 5.5 compared with pH 7.4. This might due to the hydrolysis of ester linkage between PTX and SA in PM-nano, indicating that the hydrogel possessed good stability in systemic circulation and responsiveness to releasing drugs in the tumor microenvironment.<sup>22,23</sup> The intracellular amount of PM-nano was higher than that of free drugs, indicating that utilization of supramolecular hydrogel could greatly increase the concentration of free drugs in

breast cancer cells, which might be related to the predominant cell membrane penetrability of nanostructure.<sup>13</sup> According to the cellular uptake mechanism study, PM-nano was internalized by 4T1 cells through energy-dependent caveolae-mediated endocytosis. The negligible hemolytic rate and hematological toxicity of PM-nano indicated its good biocompatibility. The pharmacokinetic results clearly indicated that MIF was successfully loaded on the PTX-SA-based hydrogel nanofiber to form an integrated nanodrug (PM-nano) with improved blood circulation and tumor accumulation performance to produce synergistic antitumor effects.

Subsequently, the effects of PM-nano on biological functions of breast cancer cells were studied. Based on the same dose of PTX, the inhibition of cell proliferation, migration, and invasion effects of nanomedicines were stronger than those of free drugs (PM-nano > PM, P-nano > P). Those with MIF were stronger than those without MIF (PM-nano > P-nano, PM > P) and those with DXM (PM > PMD > PD), while the effects of control group were the weakest. These results clearly indicated that the combination of PTX and



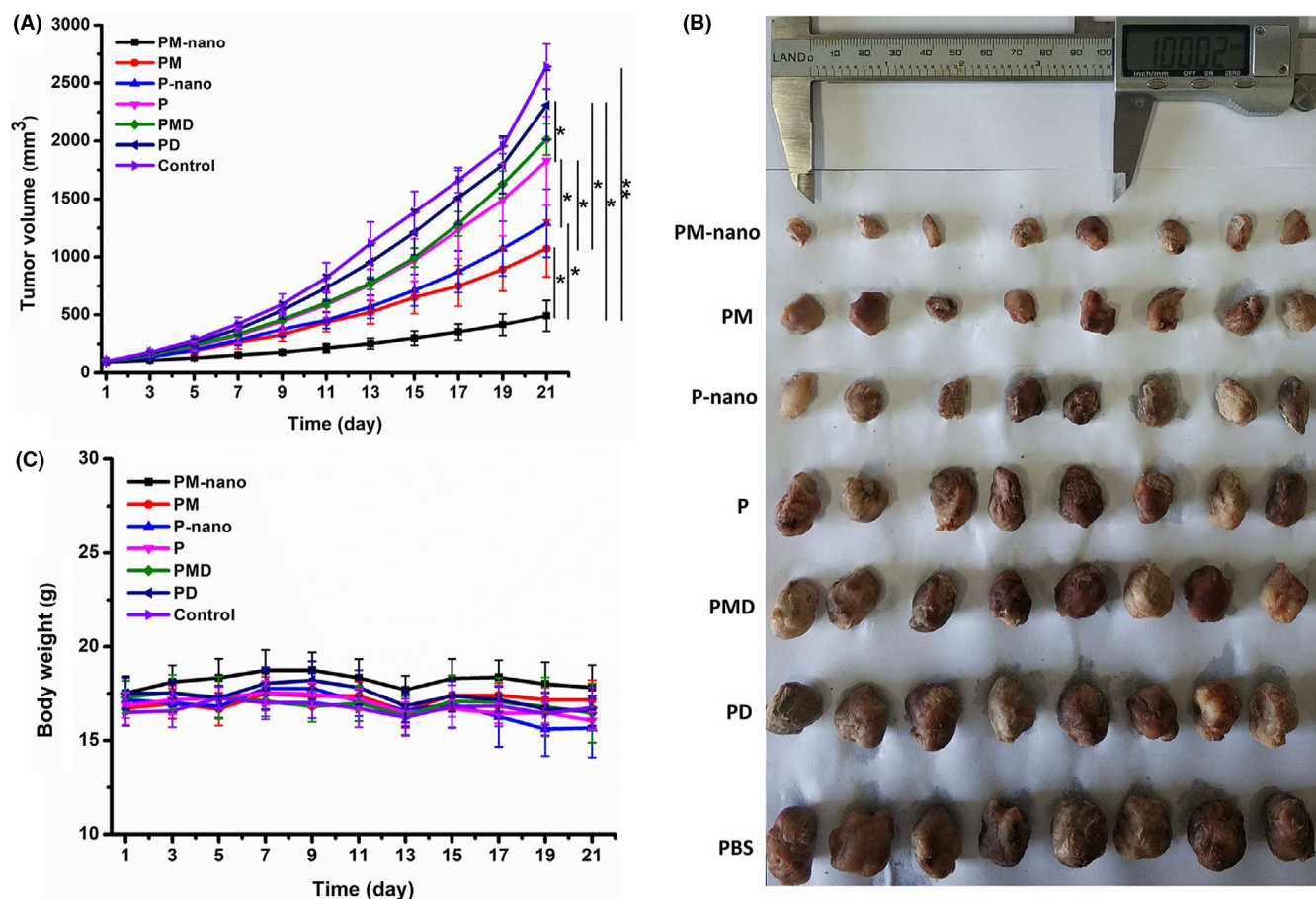


**FIGURE 6** Inhibition of tumor growth in vivo. A, Tumor volumes of mice during the whole experiment. B, Body weights of 4T1 tumor-bearing mice. C, Photographs of excised tumors on day 21 after treatment. \* $P < .05$ , \*\* $P < .01$ . P, paclitaxel; PD, paclitaxel + dexamethasone; PM, paclitaxel + mifepristone; PMD, paclitaxel + mifepristone + dexamethasone; PM-nano, paclitaxel-conjugated and mifepristone-loaded supramolecular hydrogel; P-nano, paclitaxel hydrogel

MIF through supramolecular hydrogel possessed the best anticancer activity among all groups. Similar to previous reports, the enhanced antitumor efficiency was probably attributed to the elevated cellular uptake of the nanostructured drugs, and MIF effectively antagonized DXM.<sup>4,6,24-27</sup>

Because DXM can upregulate ROR1 by GR, and ultimately promote breast cancer metastasis.<sup>4,28,29</sup> MIF can competitively bind GR and antagonize the effect of DXM.<sup>4,30,31</sup> Both MMP2 and MMP9 are upstream signals that trigger ECM remodeling and cancer metastasis, and downstream signals of many transfer-related pathways.<sup>19,31-34</sup> Many studies have shown that nanodrugs can inhibit tumor cell metastasis by downregulating the expression of MMPs.<sup>35,36</sup> In our study, the expressions of ROR1, MMP2, and MMP9 in the PM-nano group were significantly lower than in other groups, suggesting PM-nano might inhibit metastasis of breast cancer by GR/ROR1 and MMPs.

Consistent with in vitro data, PM-nano showed excellent antitumor and antimetastatic effects in mice, successively followed by the PM, P-nano, P, PD, and PBS groups. Although the brain, adrenal gland, and heart metastasis could be found through H&E staining, there was no corresponding indication in the bioluminescence

images. This might be because the cranial occlusion made the fluorescence signal difficult to capture, or the tumor lesion was too small and the fluorescence signal was too weak to be captured. However, the number of mice with metastasis indicated by the bioluminescence imaging system was highly consistent with H&E staining. Notably, similar to patients, the common metastatic sites in mice were lung, liver, and lymph node.<sup>37</sup> However, there were some rare metastases, such as heart, spleen, kidney, and adrenal gland. Therefore, doctors should pay attention to some unusual lesions in addition to the common metastatic sites during treatment and follow-up of breast cancer patients.

## 5 | CONCLUSION

In conclusion, a novel supramolecular hydrogel coloaded with PTX and MIF for breast cancer treatment was successfully prepared, in which PTX simultaneously served as drug and carrier. This hydrogel took the form of nanofibers with good water solubility, stability, satisfactory cell uptake, and fine biocompatibility. As a result, PM-nano was most effective in inhibiting the proliferation and metastasis of breast

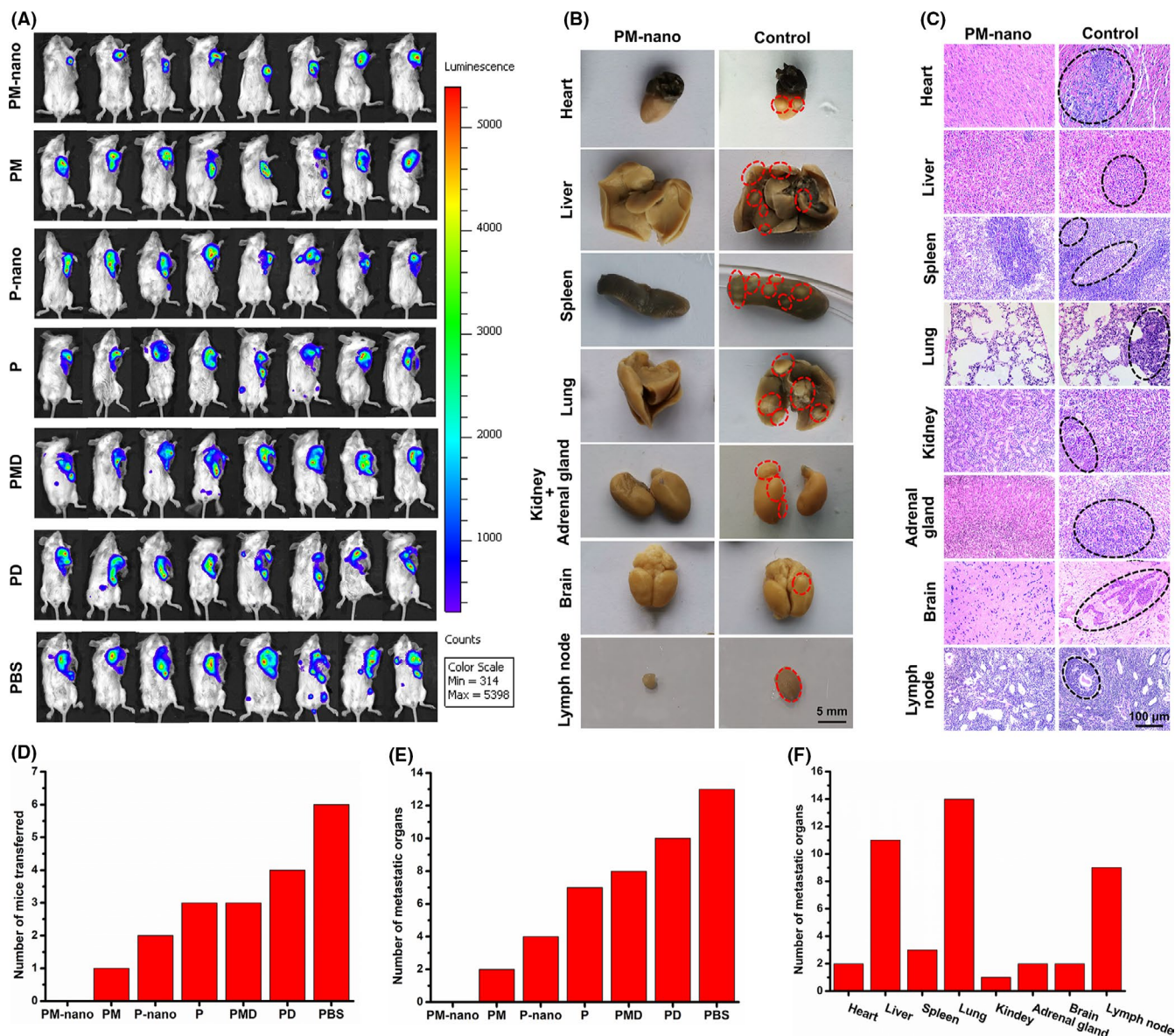


**FIGURE 7** Antimetastatic potential in vivo. A, Bioluminescence images of 4T1-Luc tumor-bearing mice on day 21 after treatment. B, C, Images of organs with and without breast cancer metastasis confirmed by gross observation (B) and H&E staining (C). The control group was defined as positive control and negative control groups, including paclitaxel + mifepristone (PM), paclitaxel hydrogel (P-nano), paclitaxel (P), paclitaxel + mifepristone + dexamethasone (PMD), paclitaxel + dexamethasone (PD), and PBS groups. D, Number of mice with metastasis in each group evaluated by pathologic analysis. E, Number of organs with metastasis in each group confirmed by pathologic analysis. F, Number of organs with metastasis in all groups detected by pathologic analysis. PM-nano, paclitaxel-conjugated and mifepristone-loaded supramolecular hydrogel

cancer cells among all groups in vitro and in vivo. The antimetastatic effect was possible through GR/ROR1 and MMPs. Therefore, our work provides a promising candidate for breast cancer therapy with remarkable antimetastatic activity and favorable biocompatibility.

#### ACKNOWLEDGMENTS

This work was supported by the National Natural Science Foundation of China (81701840), the CAMS Innovation Fund for Medical Sciences (2016-I2 M-3-022), the National Science Fund for Distinguished Young Scholars of Tianjin (18JCJQC47300), the

Non-profit Central Research Institute Fund of Chinese Academy of Medical Sciences (2018PT35031), and the Major Science and Technology Project for prevention and Treatment of major diseases in Tianjin (19ZXDBSY00090).

#### DISCLOSURE

The authors declare no potential conflict of interest.

#### ORCID

Jianfeng Liu  <https://orcid.org/0000-0003-0541-5072>



## REFERENCES

- Sung H, Ferlay J, Siegel RL, et al. Global cancer statistics 2020: GLOBOCAN estimates of incidence and mortality worldwide for 36 cancers in 185 countries. *CA Cancer J Clin*. 2021;71(3):209-249.
- Shah N, Mohammad AS, Saralkar P, et al. Investigational chemotherapy and novel pharmacokinetic mechanisms for the treatment of breast cancer brain metastases. *Pharmacol Res*. 2018;132:47-68.
- West DC, Kocherginsky M, Tonsing-Carter EY, et al. Discovery of a glucocorticoid receptor (GR) activity signature using selective GR antagonism in ER-negative breast cancer. *Clin Cancer Res*. 2018;24:3433-3446.
- Obradović MMS, Hamelin B, Manevski N, et al. Glucocorticoids promote breast cancer metastasis. *Nature*. 2019;567(7749):540-544.
- Skor MN, Wonder EL, Kocherginsky M, et al. Glucocorticoid receptor antagonism as a novel therapy for triple-negative breast cancer. *Clin Cancer Res*. 2013;19:6163-6172.
- Lee O, Choi MR, Christov K, Ivancic D, Khan SA. Progesterone receptor antagonism inhibits progesterone-related carcinogenesis and suppresses tumor cell proliferation. *Cancer Lett*. 2016;376:310-317.
- Zheng G, Shen Z, Chen H, et al. Mifepristone suppresses non-small cell lung cancer proliferation and metastasis via modulating RAS/RAF/MEK/MAPK signaling pathway. *Biomed Pharmacother*. 2017;90:437-445.
- Gao Y, Gu S, Zhang Y, et al. The architecture and function of monoclonal antibody-functionalized mesoporous silica nanoparticles loaded with mifepristone: repurposing abortifacient for cancer metastatic chemoprevention. *Small*. 2016;12(19):2595-2608.
- Fraguas-Sánchez AI, Martín-Sabroso C, Fernández-Carballido A, Torres-Suárez AI. Current status of nanomedicine in the chemotherapy of breast cancer. *Cancer Chemother Pharmacol*. 2019;84:689-706.
- Avitabile E, Bedognetti D, Ciofani G, Bianco A, Delogu LG. How can nanotechnology help the fight against breast cancer? *Nanoscale*. 2018;10:11719-11731.
- Gurunathan S, Kang MH, Qasim M, Kim JH. Nanoparticle-mediated combination therapy: two-in-one approach for cancer. *Int J Mol Sci*. 2018;19:3264.
- Li Y, Humphries B, Yang C, Wang Z. Nanoparticle-mediated therapeutic agent delivery for treating metastatic breast cancer: challenges and opportunities. *Nanomaterials (Basel)*. 2018;8:361.
- Dai Y, Xu C, Sun X, Chen X. Nanoparticle design strategies for enhanced anticancer therapy by exploiting the tumour microenvironment. *Chem Soc Rev*. 2017;46:3830-3852.
- Bakrania AK, Variya BC, Patel SS. Novel targets for paclitaxel nano formulations: hopes and hypes in triple negative breast cancer. *Pharmacol Res*. 2016;111:577-591.
- Guo P, Yang J, Liu D, et al. Dual complementary liposomes inhibit triple-negative breast tumor progression and metastasis. *Sci Adv*. 2019;5:eaav5010.
- Wang Z, Ma C, Shang Y, et al. Simultaneous co-assembly of fenofibrate and ketoprofen peptide for the dual-targeted treatment of nonalcoholic fatty liver disease (NAFLD). *Chem Commun (Camb)*. 2020;56:4922-4925.
- Ren C, Gao Y, Guan Y, et al. Carrier-free supramolecular hydrogel composed of dual drugs for conquering drug resistance. *ACS Appl Mater Interfaces*. 2019;11:33706-33715.
- Zhu L, Xi PW, Li XX, et al. The RNA binding protein RBMS3 inhibits the metastasis of breast cancer by regulating Twist1 expression. *J Exp Clin Cancer Res*. 2019;38(1):105.
- Yang HL, Thiagarajan V, Shen PC, et al. Anti-EMT properties of CoQ0 attributed to PI3K/AKT/NFKB/MMP-9 signaling pathway through ROS-mediated apoptosis. *J Exp Clin Cancer Res*. 2019;38(1):186.
- Li F, Lu J, Liu J, et al. A water-soluble nucleolin aptamer-paclitaxel conjugate for tumor-specific targeting in ovarian cancer. *Nat Commun*. 2017;8:1390.
- Guo Q, Liu Y, Wang Z, et al. Supramolecular nanofibers increase the efficacy of 10-hydroxycamptothecin by enhancing nuclear accumulation and depleting cellular ATP. *Acta Biomater*. 2021;122:343-353. doi:10.1016/j.actbio.2020.12.052
- Yang L, Zhang C, Huang F, et al. Triclosan-based supramolecular hydrogels as nanoantibiotics for enhanced antibacterial activity. *J Control Release*. 2020;324:354-365.
- Xu H, Lu X, Li J, et al. Superior antitumor effect of extremely high drug loading self-assembled paclitaxel nanofibers. *Int J Pharm*. 2017;526:217-224.
- Liu R, Shi P, Nie Z, et al. Mifepristone suppresses basal triple-negative breast cancer stem cells by down-regulating KLF5 expression. *Theranostics*. 2016;6:533-544.
- Reeder A, Attar M, Nazario L, et al. Stress hormones reduce the efficacy of paclitaxel in triple negative breast cancer through induction of DNA damage. *Br J Cancer*. 2015;112:1461-1470.
- Sorrentino G, Ruggeri N, Zannini A, et al. Glucocorticoid receptor signalling activates YAP in breast cancer. *Nat Commun*. 2017;8:14073.
- Wan X, Beaudoin JJ, Vinod N, et al. Co-delivery of paclitaxel and cisplatin in poly(2-oxazoline) polymeric micelles: implications for drug loading, release, pharmacokinetics and outcome of ovarian and breast cancer treatments. *Biomaterials*. 2019;192:1-14.
- Zhang S, Zhang H, Ghia EM, et al. Inhibition of chemotherapy resistant breast cancer stem cells by a ROR1 specific antibody. *Proc Natl Acad Sci USA*. 2019;116(4):1370-1377.
- Cao J, Wang X, Dai T, et al. Twist promotes tumor metastasis in basal-like breast cancer by transcriptionally upregulating ROR1. *Theranostics*. 2018;8:2739-2751.
- Cui B, Zhang S, Chen L, et al. Targeting ROR1 inhibits epithelial-mesenchymal transition and metastasis. *Cancer Res*. 2013;73:3649-3660.
- Senthil Kumar KJ, Gokila Vani M, Hsieh HW, et al. MicroRNA-708 activation by glucocorticoid receptor agonists regulate breast cancer tumorigenesis and metastasis via downregulation of NF-kappaB signaling. *Carcinogenesis*. 2019;40:335-348.
- Chen Q, Zhang JJ, Ge WL, et al. YY1 inhibits the migration and invasion of pancreatic ductal adenocarcinoma by downregulating the FER/STAT3/MMP2 signaling pathway. *Cancer Lett*. 2019;463:37-49.
- Brabletz T, Kalluri R, Nieto MA, Weinberg RA. EMT in cancer. *Nat Rev Cancer*. 2018;18(2):128-134.
- Pastushenko I, Blanpain C. EMT transition states during tumor progression and metastasis. *Trends Cell Biol*. 2019;29:212-226.
- Lv Y, Zhao X, Zhu L, et al. Targeting intracellular MMPs efficiently inhibits tumor metastasis and angiogenesis. *Theranostics*. 2018;8(10):2830-2845.
- Wang K, Ye H, Zhang X, et al. An exosome-like programmable-bioactivating paclitaxel prodrug nanoplatfor for enhanced breast cancer metastasis inhibition. *Biomaterials*. 2020;257:120224.
- Yates LR, Knappskog S, Wedge D, et al. Genomic evolution of breast cancer metastasis and relapse. *Cancer Cell*. 2017;32:169-184.e7.

## SUPPORTING INFORMATION

Additional supporting information may be found in the online version of the article at the publisher's website.

**How to cite this article:** Zhao C-C, Zhang C-G, Sun X, et al. Paclitaxel-based supramolecular hydrogel loaded with mifepristone for the inhibition of breast cancer metastasis. *Cancer Sci*. 2022;113:733-743. doi:10.1111/cas.15230